Nonlinear response theory for time-periodic elongational flows

B. D. Todd
Cooperative Research Centre for Polymers, CSIRO Molecular Science, Bag 10, Clayton South, Victoria 3169, Australia
(Received 3 February 1998; revised manuscript received 2 July 1998)

The time-dependent nonlinear response theory of Petravic and Evans [Phys. Rev. Lett. **78**, 1199 (1997); Phys. Rev. E **56**, 1207 (1997)] is applied to the case of an atomic fluid undergoing oscillatory elongational flow. It is found that nonlinear response calculations agree very well with direct nonequilibrium molecular dynamics calculations of the diagonal elements of the pressure tensor. At very weak applied fields, nonlinear response theory is statistically superior to the direct calculation, which suffers from low signal to noise ratios, but at higher fields direct averaging of phase variables is observed to be superior. [S1063-651X(98)12210-9]

PACS number(s): 61.20.Ja, 05.20.−y, 66.20.+d, 83.50.Jf

I. INTRODUCTION

Elongational flow is a difficult rheological problem to study by the use of molecular dynamics techniques. The main problem with such calculations is the requirement that the periodic boundary conditions evolve in time such that they remain compatible with the equations of motion. For planar shear flow this is not a problem, as the flow geometry guarantees that the boundary conditions remain periodic for theoretically infinite simulation times. However, for elongational flow this convenient geometry is destroyed. Elongational flow occurs when a fluid is stretched in at least one direction, and compressed in at least another. This implies that the simulation cell dimensions must either increase or decrease in length. Eventually the simulation must cease when the length of the simulation cell in the compressing direction reaches its minimum extension of twice the interaction potential cutoff radius. For relatively simple fluids this is not a serious concern, as previous studies [1–4] have shown that the fluid will reach steady state before the maximum simulation time is reached. However, this will not be the case for more complex molecular fluids, where now the relaxation times of the fluid will exceed the maximum allowable simulation time in all but the weakest of flows [5]. It is primarily for this reason that few nonequilibrium molecular dynamics (NEMD) studies of elongational flow have been attempted in the past decade.

There have been several recent attempts to overcome this technical difficulty. Baranyai and Cummings [4] devised a method of increasing the total simulation time available by effectively doubling the cell length in the contracting dimension when it was close to the minimum length. This was accomplished by defining one set of images as real particles and adding random displacements to their positions and velocities. Since the overall system is a nonlinear dynamical one, the phase-space trajectories of the new particles will be uncorrelated with the original particles after a characteristic time determined by the magnitude of the Lyapunov exponent. However, if the elongation rate is very high there is no time for the new particles to evolve along a substantially different trajectory. It was found that for their system of simple Weeks, Chandler, and Anderson (WCA) atoms [6], this doubling scheme could only be used for elongation rates <0.5 in reduced units.

Recently Todd and Daivis [7] devised a NEMD method that applies an oscillating strain rate to the equations of motion for a simple atomic fluid. This ensures that the system attains a temporally periodic steady state. For a given magnitude of the strain rate, quantities of interest, such as the diagonal elements of the pressure tensor, and hence elongational viscosities, are then calculated by extrapolating their frequency dependent values down to zero frequency. The main advantage of this technique is that it provides a convenient and consistent means of extrapolating to the zero frequency (steady elongation) elongational viscosity, unlike the standard method, in which it may be difficult to distinguish between the transient response and the steady-state response. The method also enables one to study the frequency dependence of the elongational viscosity, and thus probe the rich visco-elastic behavior of fluids subject to elongation [8].

In another attempt to address this problem of finite simulation time, Todd [9] applied time-independent nonlinear response theory, in the form of the transient time correlation functions (TTCF) of Morriss and Evans [10], to a fluid undergoing steady elongational flow. The advantage of this approach is that TTCF is much more efficient at low field strengths than direct averaging, and as the total simulation time for elongational flow is inversely proportional to the field strength (i.e., the applied strain rate), the simulation can be run for much longer times than could otherwise be possible. As molecular fluids display significant non-Newtonian behavior at relatively low strain rates, the method could be useful for studying their rheology under elongational flow. The method has another surprisingly beneficial feature in that it does not detect any transient oscillations in the pressure. This in turn allows more accurate determinations of the genuine long-time steady-state response of the fluid to an applied time-independent field.

The work performed in this paper essentially represents a synthesis of the previous two methods described above [7,9]. The method of Todd and Daivis [7] is restricted to values of the applied strain of $\sim\geqslant 0.1$. Below this value the signal to noise ratio deteriorates significantly, making the conventional direct averaging procedure unfeasible. Petravic and Evans [11] have recently shown that time-dependent nonlinear response theory can be successfully applied to systems that are driven by a time-periodic external field. The motivation for this current work is to apply Petravic and Evans' method to the oscillatory system of Todd and Daivis, thus

allowing access to rheological information at strain rates normally inaccessible by conventional direct NEMD methods.

II. THEORY

Petravic and Evans [11] based their time-dependent nonlinear response theory on the TTCF method of Morriss and Evans [10]. They showed that for a system of particles under the influence of an external time-periodic field, subject to a Gaussian isokinetic constraint, the ensemble average of any arbitrary phase variable B is given as

$$\langle B[\mathbf{\Gamma}(t;\varphi(t)=\varphi_p)]\rangle = \langle B[\mathbf{\Gamma}(0;\varphi(0)=\varphi_p)]\rangle - \beta\int_0^t ds F^e(\varphi_p-\omega s) \times\langle B[\mathbf{\Gamma}(s;\varphi(s)=\varphi_p)]J[\mathbf{\Gamma}(0;\varphi(0)=\varphi_p-\omega s)]\rangle, \quad (1)$$

where $\beta=1/kT$, k is Boltzmann's constant, φ is a phase angle in the generalized phase space defined by $\mathbf{\Gamma}'=(\mathbf{\Gamma},\varphi)$, φ_p is an arbitrary constant value of this phase angle, F^e is the external driving field of frequency ω, and J is the dissipative flux.

It is absolutely essential to understand the meaning of Eq. (1), and because of this some time will be devoted here to its interpretation before proceeding any further. Although it is in a form similar to the corresponding time-independent TTCF expression, there are subtle differences in interpretation of the symbols that are not intuitively obvious.

Time-dependent TTCF makes use of an abstract notion of an ''extended phase space,'' $\mathbf{\Gamma}'=(\mathbf{\Gamma},\varphi)=(\mathbf{q}_i,\mathbf{p}_i,\varphi_i;i=1,...,N)$. To make sense of this, consider an ensemble of Π ''daughter'' nonequilibrium phase space trajectories, each one originating at $t=0$ from an equilibrium ''mother'' trajectory. Each daughter is initiated with different phase angles, as depicted in Fig. 1(a). In this paper each separate time origin along the equilibrium mother trajectory is referred to as a node. One can consider this entire set of phase-space trajectories belonging to a *single* extended phase space. One could follow the time evolution of any arbitrary phase variable B in this *extended* phase space, and plot the value of $B[\mathbf{\Gamma}(t;\varphi(t)=\varphi_p)]$ as a function of time, as illustrated in Fig. 1(b). In this example, a set of four nonequilibrium trajectories [curves $(i)-(iv)$] are initiated at a node, each with a different value of the initial phase angle of the driving field $\varphi(0)$. If one were interested in the values of $B(t)$ evaluated at only specific *constant* values of the phase angle φ_p, then one could, on a single graph, plot this value of $B[\mathbf{\Gamma}(t;\varphi(t)=\varphi_p)]$ for each of the four trajectories, as indicated in curve (v). One would find that $B[\mathbf{\Gamma}(t;\varphi(t)=\varphi_p)]$ experiences an initial transient stage from $t=0$ (i.e., when the field is switched on) up to some time $t=t_s$. At times $t>t_s$, the value of $B[\mathbf{\Gamma}(t;\varphi(t)=\varphi_p)]$ is constant, indicating that a temporally periodic nonequilibrium steady state has been reached. This is analogous to the case of following the traditional phase space trajectory of a *single* system under the influence of a time-independent field; in this case $B(t)$ will also experience an initial transient stage before reaching its steady-state value after some time t_s. Indeed, it is precisely this analogy that allows one to derive Eq. (1) in the first place; it relies on the fact that any phase

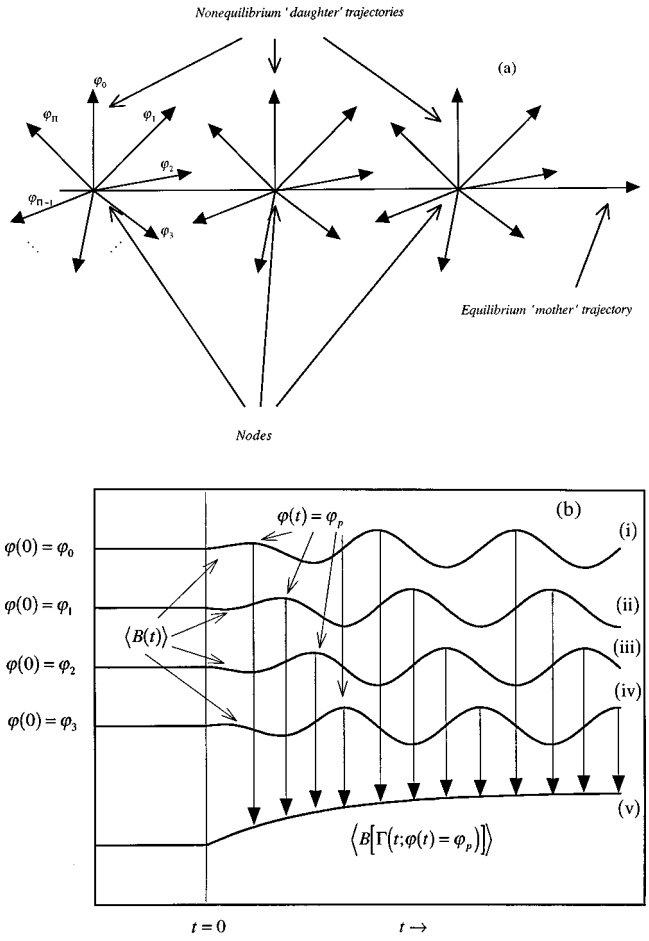

FIG. 1. (a) Schematic representation of extended phase space. (b) Time evolution of $B[\mathbf{\Gamma}(t;\varphi(t)=\varphi_p)]$ generated from a set of nonequilibrium trajectories commencing at different initial values of φ.

variable in extended phase space, measured at a *constant* value of the phase angle φ_p, will always attain a ''steady state'' under the application of a time-periodic driving external field. It is this correspondence that makes Eq. (1) so similar in form to the time-independent TTCF expression.

With an appreciation of the notion of extended phase space, we now consider the interpretation of the symbols under the integral sign, and indeed the interpretation of the integration itself. Again this is more easily explained pictorially, with the aid of Fig. 2.

Consider a system which is driven by a time-periodic field $F^e(t,\varphi_0)$, such that $F^e(t,\varphi_0)=F^e(t+\tau,\varphi_0)$, where τ is the period and φ_0 is an initial phase angle. Furthermore, let $\tau=6\,\delta t$, as depicted in Fig. 2, where δt is the evolution time step. The vertical and horizontal axes of the cells represent time and phase angle evolutions of any arbitrary phase variable B, respectively. In this specific example, we are interested in the evolution of a trajectory that has commenced at $t=0$ with an initial phase angle $\varphi_0=2\,\omega\,\delta t$. Even though we are only interested in calculating the nonlinear response for this one trajectory, the TTCF method of Petravic and Evans [11] demands that a number of *different* nonequilibrium trajectories be allowed to evolve, each starting at $t=0$ with different initial phase angles φ_0 such that they span the entire range of $\varphi\in[0,\Phi_\tau]$, where $\Phi_\tau=\omega\tau$. For the purposes of illustration only, this range is divided into six discrete angles

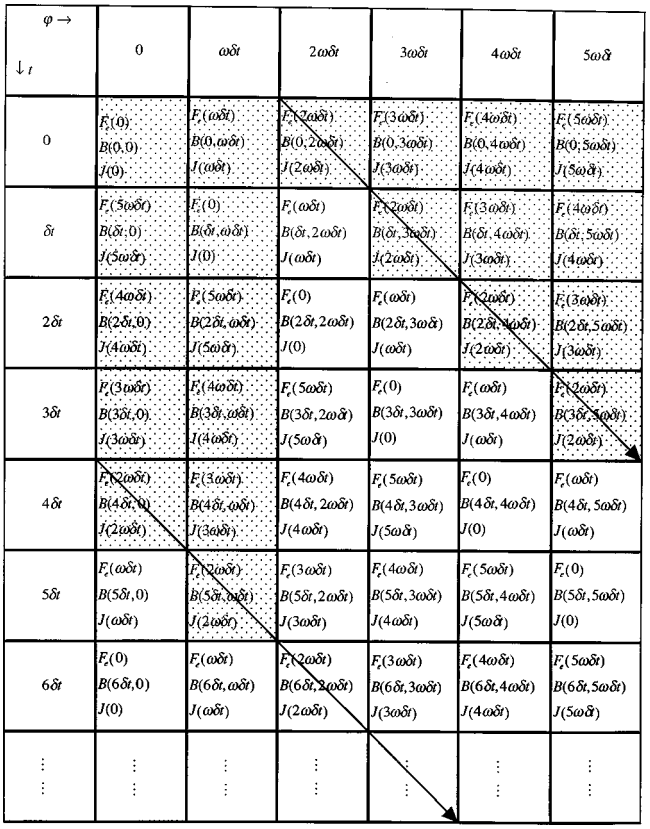

FIG. 2. Schematic representation of Eq. (1). The example is periodic in time, with period $\tau = 6\,\delta t$.

in Fig. 2, each separated by $\omega\,\delta t$, though in practice one would need a larger set of discrete angles spanning $[0,\Phi_\tau]$. In such a pictorial scheme each distinct nonequilibrium trajectory in the extended phase space would be represented by a diagonal arrow in a matrix of cells, commencing at $(t,\varphi) = (0,\varphi_0)$ and moving down and to the right. Specific to our example, the arrow commences at the point $(t,\varphi)=(0,2\omega\delta t)$. As molecular dynamics simulations evolve with discrete incremental time steps of δt, each contiguous diagonal cell represents a forward advance in time of δt, and in phase angle of $\omega\,\delta t$, over the previous one. In addition, each cell depicts the *product* of B at time t and phase angle $\varphi(t)$, with the values of the external field and the dissipative flux evaluated at $t=0$, i.e., $F^e(0,\varphi(0)=\varphi_0)B[\mathbf{\Gamma}(t;\varphi(t))]J[\mathbf{\Gamma}(0;\varphi(0) = \varphi_0)]$. However, the integration that appears in Eq. (1) *is not* along the diagonal (i.e., *not* along the single trajectory indicated by the arrow); rather it is down the columns of Fig. 2, from $s=0$ up to any desired value of the time, $s=t$. The integration occurs *only* for those values of B that are evaluated at a constant value of the phase angle $\varphi(t)=\varphi_p$. For example, if one wanted to calculate the value of $\langle B[\mathbf{\Gamma}(t = 3\,\delta t;\varphi(t)=5\,\omega\,\delta t)]\rangle$ using the TTCF formalism, one would integrate over (i.e., sum) each of the shaded squares in the last column of Fig. 2 and average over the total number of nodes. Doing this for each value of t would produce TTCF values of $\langle B[\mathbf{\Gamma}(t;\varphi(t)=\varphi_p)]\rangle$ that correspond to the direct values generated for curve (v) of Fig. 1(b).

It is essential to realise that each value of $B[\mathbf{\Gamma}(t;\varphi(t) = \varphi_p)]$ in any one column of Fig. 2 originates from an independent, *separate*, trajectory in the full ensemble of extended phase space. Equation (1) represents an integration along *contiguous* trajectories that originate from different initial values of the phase angle $\varphi_0=\varphi_p-\omega s$. Note that the field and dissipative flux are evaluated at $t=0$ and $\varphi=\varphi_0$ for each individual trajectory, which is why they are represented as $F^e(\varphi_p-\omega s)$ and $J[\mathbf{\Gamma}(0;\varphi(0)=\varphi_p-\omega s)]$ in Eq. (1). As is the case with time-independent TTCF the first term on the right-hand side of Eq. (1) simply represents the ensemble average of the equilibrium value of B at $t=0$. Note that the cells themselves are depicted in Fig. 2 as periodic, with period τ. Thus, one only needs to generate trajectories that span the extended phase space $(\mathbf{\Gamma},\varphi)$, where $\varphi\in[0,\Phi_\tau]$. In our example $6\,\omega\,\delta t=\Phi_\tau$, hence the diagonal arrow corresponding to a single trajectory repeats itself from the left of the matrix whenever $\mathrm{mod}[\varphi(t),6\omega\,\delta t]=0$. Finally, to generate a complete picture of the evolution of B as a function of time and phase angle, one evaluates Eq. (1) for each value of φ_p, as indicated by the shaded cells in Fig. 2. In this specific example the TTCF method would yield the values of $\langle B[\mathbf{\Gamma}(t;\varphi(t))]\rangle$ for all times up to $t=5\,\delta t$, although of course one can, in principle, continue integrating up to $t \to\infty$. Even though our example has been confined to calculating $\langle B[\mathbf{\Gamma}(t;\varphi(t))]\rangle$ for a nonequilibrium system with initial phase angle $\varphi_0=2\,\omega\,\delta t$, clearly we have all the information we need to calculate $\langle B[\mathbf{\Gamma}(t;\varphi(t))]\rangle$ for *any* nonequilibrium system commencing at $t=0$ with any φ_0; thus one can extract an enormous amount of information from a single set of simulation data in the full extended phase space.

With the interpretation of Eq. (1) clarified, it is a relatively straightforward process to extend the theory to the case of elongational flow. In a previous paper [9] it was demonstrated how to do this for time-independent elongational flow. Essentially the same procedure carries over to the case of time-dependent flow. In short, the task is to generalize Eq. (1) for any arbitrary flow, and then identify the values of F^e and J for any specific elongational flow.

By applying the derivation of Petravic and Evans [11] to any arbitrary generalized flow characterized by a tensorial external field $\mathbf{F}^e(\varphi)$ and dissipative flux $\mathbf{J}(\mathbf{\Gamma})$, one can readily show that the general expression for the nonlinear response of any phase variable $B[\mathbf{\Gamma}(t;\varphi(t)=\varphi_p)]$ is given as

$$\begin{aligned}\langle B[\mathbf{\Gamma}(t;\varphi(t)=\varphi_p)]\rangle &= \langle B[\mathbf{\Gamma}(0;\varphi(0)=\varphi_p)]\rangle \\ &\quad -\beta\sum_{\delta,\sigma}\int_0^t ds F^e_{\delta\sigma}(\varphi_p-\omega s) \\ &\quad \times\langle B[\mathbf{\Gamma}(s;\varphi(s)=\varphi_p)] \\ &\quad \times J_{\sigma\delta}[\mathbf{\Gamma}(0;\varphi(0)=\varphi_p-\omega s)]\rangle, \qquad (2)\end{aligned}$$

where δ, σ range over all Cartesian dimensions.

For an atomic fluid undergoing planar shear flow, the adiabatic time derivative of the internal energy H_0, is usually written as $\dot H_0 = -JF^e$, where J and F^e are as previously defined. For more complex flows, one can generalize this to $\dot H_0 = -\mathbf{J}:\mathbf{F}^e$, where now both $\mathbf{J}$ and $\mathbf{F}^e$ are tensorial quantities as described above. For planar shear (or planar Couette) flow, it is easily seen that $\dot H_0 = -\dot\gamma P_{xy} V$ [12], where $\dot\gamma$ is the strain rate, P_{xy} is the xy element of the pressure tensor (negative of the shear stress), and V is the system volume.

For oscillatory elongational flow, $\mathbf{F}^e$ can be expressed as an applied time-dependent strain rate tensor,

$$\mathbf{F}^e(\varphi)\equiv\nabla\mathbf{u}(\varphi)=\begin{pmatrix}\dot{\varepsilon}_{xx} & 0 & 0\\ 0 & \dot{\varepsilon}_{yy} & 0\\ 0 & 0 & \dot{\varepsilon}_{zz}\end{pmatrix}\cos(\varphi)\equiv\dot{\underline{\underline{\varepsilon}}}\cos(\varphi), \quad (3)$$

where $\mathbf{u}$ is the streaming velocity of the fluid and $\dot{\epsilon}_{\alpha\alpha}$ is the elongational strain rate defined as $\partial u_\alpha/\partial_\alpha$, where $\alpha=x,y,z$. Here the explicit time dependence of the field has been transformed into a dependence on an extended phase-space variable, namely, the phase angle, $\varphi=\omega t+\varphi_0$. Assuming pairwise additive potential interactions between atoms, the total internal energy of a particle is given as

$$H_i=\frac{\mathbf{p}_i^2}{2m_i}+\tfrac{1}{2}\sum_j \phi_{ij}, \quad (4)$$

where the momenta, $\mathbf{p}_i$ are peculiar with respect to $\mathbf{u}$. The total internal energy is thus $H_0=\Sigma_i H_i$. Assuming unthermostatted extended Sllod equations of motion for the particle dynamics [7,11,12],

$$\dot{\mathbf{r}}_i=\frac{\mathbf{p}_i}{m_i}+\mathbf{r}_i\cdot\nabla\mathbf{u}(\varphi),$$

$$\dot{\mathbf{p}}_i=\mathbf{F}_i-\mathbf{p}_i\cdot\nabla\mathbf{u}(\varphi),$$

$$\dot{\varphi}=\omega, \quad (5)$$

the adiabatic time derivative of the total internal energy is given as

$$\dot{H}_0=-[\dot{\varepsilon}_{xx}P_{xx}+\dot{\varepsilon}_{yy}P_{yy}+\dot{\varepsilon}_{zz}P_{zz}]\cos(\varphi)V$$
$$=-[V\mathbf{P}:\nabla\mathbf{u}(\varphi)]\equiv-\mathbf{J}:\mathbf{F}^e(\varphi). \quad (6)$$

As it is these values of $\mathbf{J}$ and $\mathbf{F}^e$ that must be substituted into Eq. (2), one obtains the time-dependent TTCF expression for the time evolution of any arbitrary phase variable $B(t)$ at a constant value of the phase angle φ_p,

$$\langle B[\mathbf{\Gamma}(t;\varphi(t)=\varphi_p)]\rangle=\langle B[\mathbf{\Gamma}(0;\varphi(0)=\varphi_p)]\rangle$$
$$-\beta V\Bigg(\dot{\varepsilon}_{xx}\int_0^t ds\,\cos(\varphi_p-\omega s)\langle B[\mathbf{\Gamma}(s;\varphi(s)=\varphi_p)]P_{xx}[\mathbf{\Gamma}(0;\varphi(0)=\varphi_p-\omega s)]\rangle$$
$$+\dot{\varepsilon}_{yy}\int_0^t ds\,\cos(\varphi_p-\omega s)\langle B[\mathbf{\Gamma}(s;\varphi(s)=\varphi_p)]P_{yy}[\mathbf{\Gamma}(0;\varphi(0)=\varphi_p-\omega s)]\rangle$$
$$+\dot{\varepsilon}_{zz}\int_0^t ds\,\cos(\varphi_p-\omega s)\langle B[\mathbf{\Gamma}(s;\varphi(s)=\varphi_p)]P_{zz}[\mathbf{\Gamma}(0;\varphi(0)=\varphi_p-\omega s)]\rangle\Bigg). \quad (7)$$

Since we are only concerned in this work with calculating the diagonal elements of the pressure tensor, $P_{\delta\delta}$ (where $\delta=x$, y, or z), we simply replace B with $P_{\delta\delta}$ in Eq. (7). It is these elements that are directly related to the elongational viscosity [7,8], and are hence of significant rheological interest.

III. SIMULATIONS

The thermostated *extended* phase-space Sllod (so named because of its close relationship to the Dolls tensor algorithm) equations of motion [7,11,12] that are used in this work are

$$\dot{\mathbf{r}}_i=\frac{\mathbf{p}_i}{m_i}+\mathbf{r}_i\cdot\nabla\mathbf{u}(\varphi),$$

$$\dot{\mathbf{p}}_i=\mathbf{F}_i-\mathbf{p}_i\cdot\nabla\mathbf{u}(\varphi)-\alpha\mathbf{p}_i,$$

$$\dot{\varphi}=\omega, \quad (8)$$

where α is a Gaussian thermostat multiplier used to constrain the system to constant temperature, given as

$$\alpha=\frac{\sum_i \mathbf{p}_i\cdot[\mathbf{F}_i-[\mathbf{p}_i\cdot\nabla\mathbf{u}(\varphi)]]}{\sum_i \mathbf{p}_i^2}. \quad (9)$$

As previously mentioned, the periodic boundary conditions will evolve in time in an oscillatory manner. Integrating the equations of motion shows that the dimensions of the simulation cell change exponentially, but periodically,

$$L_\delta(t)=L_\delta(0)\exp(\dot{\varepsilon}_{\delta\delta}\omega^{-1}[\sin(\omega t+\varphi_0)-\sin\,\varphi_0]), \quad (10)$$

where $L_\delta(t)$ is the length of the simulation cell at time t in the direction $\delta(\delta=x,y,z)$. The value of ω can be chosen judiciously so that it is never less than the minimum frequency allowable for a given magnitude of the elongational strain rate,

$$\omega_{\min}=2\left|\frac{\max(\dot{\varepsilon}_{\delta\delta})}{\ln\left(\frac{2r_c}{L_\delta(0)}\right)}\right|, \quad (11)$$

where r_c is the cutoff potential radius. Any value of the frequency less than $\omega_{\min}$ will result in $L_\delta(t)<2r_c$ for at least one of the extended phase-space trajectories that spans φ

$\in[0,2\pi]$, which is not allowable. We also note that, for constant volume, at least two dimensions must oscillate in time, either expanding or contracting such that the total volume of the system is preserved [i.e., $\mathrm{Tr}(\nabla \mathbf{u})=0$].

Simulations are performed on three kinds of oscillatory elongational flow: planar elongational flow (PEF), uniaxial stretching flow (USF), and biaxial stretching flow (BSF). PEF occurs when one of the diagonal elements in the strain rate tensor is zero, and the other two are equal in magnitude and opposite in sign (stretching and compressing). USF implies one element is positive (stretching) and the other two are negative (compressing) and of half the magnitude, while for BSF one element is negative (compressing) and the other two are positive (stretching) and of half the magnitude. These types of flows ensure that the system volume is a constant of the motion. Actually, USF and BSF simulations are equivalent for oscillatory elongational flow. This is because any particular cell dimension will expand for one-half of the period and contract for the other half. If one then extrapolates frequency-dependent values to zero frequency, one can obtain all the information one needs for steady-elongation BSF-USF flows in a single oscillatory experiment. This is useful, for example, if one is interested in the zero-frequency elongational viscosity, but the technique can also be used to calculate frequency-dependent viscosities [7,8].

For the geometry used in this work, PEF implies $\dot{\varepsilon}_{xx}=-\dot{\varepsilon}$, $\dot{\varepsilon}_{yy}=\dot{\varepsilon}$, $\dot{\varepsilon}_{zz}=0$, and BSF-USF implies $\dot{\varepsilon}_{xx}=\dot{\varepsilon}$, $\dot{\varepsilon}_{yy}=-\frac{1}{2}\dot{\varepsilon}$, $\dot{\varepsilon}_{zz}=-\frac{1}{2}\dot{\varepsilon}$ (or, equivalently, $\dot{\varepsilon}_{xx}=-\dot{\varepsilon}$, $\dot{\varepsilon}_{yy}=\frac{1}{2}\dot{\varepsilon}$, $\dot{\varepsilon}_{zz}=\frac{1}{2}\dot{\varepsilon}$).

The simulation cell consisted of $N=108$ atoms that interact via the WCA potential of Weeks, Chandler, and Andersen [6] defined as $\phi(r)=4(r^{-12}-r^{-6})+1$ for $r<2^{1/6}$; $\phi(r)=0$, for $r>2^{1/6}$, where the WCA potential constants σ and ε, as well as the mass of the atoms and Boltzmann's constant, are defined to be unity for simplicity, and therefore all measured properties are in dimensionless reduced units. The system is three dimensional, and is periodic in all dimensions. All simulations are performed at the Lennard-Jones triple point, $\rho=0.8442$ and $T=0.722$. The equations of motion were integrated using a fourth-order Runge-Kutta scheme, and the integration timestep ranged between 0.001-0.004 in reduced units for all simulations.

The size of the equilibrium cell was $L_x=L_y=L_z=(N/\rho)^{1/3}=5.0388$. In all simulations, an equilibrium ''mother'' trajectory was maintained at a constant-state point of $(\rho,T)=(0.8442,0.722)$, while at equal intervals a few hundred time steps apart, a sufficient number of nonequilibrium ''daughter'' trajectories were initiated to span the entire extended phase space angle, $\varphi\in[0,2\pi]$ (see Fig. 1). This time separation was chosen to ensure that contiguous nonequilibrium trajectories originating from different nodes were uncorrelated.

Morriss and Evans [10] demonstrated that for planar shear simulations, a substantial improvement in the signal to noise ratio at long times can be obtained through prudent phase-space symmetry mappings. This mapping scheme was later extended to incorporate elongational flow [9], and the same scheme is used in this work. For PEF simulations a suitable mapping is $\mathbf{\Gamma}_1\rightarrow\mathbf{\Gamma}_2$, where $\mathbf{\Gamma}_1=(x_i,y_i,z_i,p_{xi},p_{yi},p_{zi})$, $\mathbf{\Gamma}_2=(y_i,x_i,z_i,p_{yi},p_{xi},p_{zi})$. This mapping has the necessary

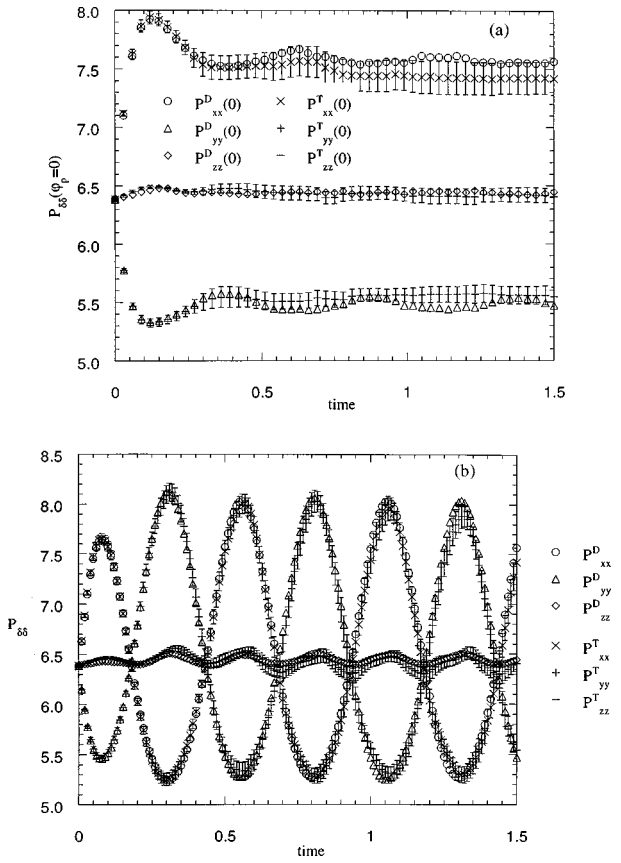

FIG. 3. (a) Direct (D) and TTCF (T) values of $\langle P_{\delta\delta}[\mathbf{\Gamma}(t;\varphi_p=0)]\rangle$ for a PEF simulation with an applied strain rate of $\dot{\varepsilon}_{xx}=-0.5$, $\dot{\varepsilon}_{yy}=0.5$, $\dot{\varepsilon}_{zz}=0$, and frequency of $\omega=12.566$. Error bars for direct pressures are smaller than the plotting symbol characters. (b) Direct and TTCF pressures for the system in (a).

requirements that it preserves the total internal energy of the equilibrium system at $t=0$, while ensuring at the same time that the new nonequilibrium trajectory ($\mathbf{\Gamma}_2$) evolves along a distinct path to the original nonequilibrium trajectory ($\mathbf{\Gamma}_1$). For BSF/USF flows, two initial equilibrium phases are insufficient for zeroing the long time fluctuations, and an additional phase-space mapping, $\mathbf{\Gamma}_1\rightarrow\mathbf{\Gamma}_3$, where $\mathbf{\Gamma}_3=(z_i,y_i,x_i,p_{zi},p_{yi},p_{xi})$, is required. Neither of these schemes are unique, or exhaustive, but they are sufficient.

IV. RESULTS AND DISCUSSION

The results of an oscillating PEF simulation with $\dot{\varepsilon}_{xx}=-0.5$, $\dot{\varepsilon}_{yy}=0.5$, $\dot{\varepsilon}_{zz}=0$ are shown in Figs. 3(a) and 3(b). These results consisted of data averaged over a total of $10\times2\times200\times50$ NEMD trajectories (i.e., 10 separate runs of two phase-space mappings of 200 nodes of 50 discrete phase angles spanning the range $\varphi\in[0,2\pi]$). The frequency of the applied strain rate was $\omega=12.566$, which corresponds to a period of $\tau=0.5$ reduced time units. The frequency is high enough to ensure that $L_\delta(t)\gg 2r_c$, and hence that simulation artifacts induced by small box dimensions are minimized. Each NEMD trajectory was run for a total length of 3τ time steps.

Figure 3(a) shows $P_{\delta\delta}$ (where $\delta=x$, y, or z) as a function of time at a constant phase angle of $\varphi_p=0$. The TTCF values are calculated by Eq. (7), and are compared with the direct

time-averaged results. One observes an initial period where the fluid relaxes to a nonequilibrium ''steady state'' at approximately $t=0.35$, after which the pressure (at constant φ_p) is essentially constant, though there is evidence of weak oscillations in the direct pressures. In fact, plotting the pressure in this manner is a very useful tool for checking if the fluid has attained a genuine time-periodic steady state. A plot of the pressure itself would, of course, oscillate with period τ, and it is not as obvious to determine when a time-periodic steady state has been reached.

Both the direct (D) and TTCF (T) results are in excellent agreement with each other. This represents the first independent check that the method of Petravic and Evans [11] is indeed valid, and will work for generalized flows. However, contrary to Petravic and Evans, the direct results are more efficient for this relatively high strain rate than the TTCF results (the error bars for the direct results are smaller than the plotting symbol size). In their work Petravic and Evans found that time-dependent TTCF was more efficient than direct averaging for high or low strain rate rates (contrary to time-independent TTCF, which is known to be more efficient only at low strain rates [9,10]). A possible reason for this is the difference in system size of the current work compared with that of Petravic and Evans. In their simulations they only considered a two-particle system, where naturally the statistical noise in the direct calculations would have been significantly worse than in this work, where the number of particles is 108. Thus it is likely that for very small system sizes, time-dependent TTCF is at least as efficient as direct averaging, but that this is not necessarily true as the number of particles in the simulation cell increases.

Of further interest in Fig. 3(a) is the similarity of $P_{\delta\delta}(\varphi=\varphi_p)$ with $P_{\delta\delta}$ in the time-independent TTCF studies of elongational flow previously done [9]. A comparison of both results in fact stresses the point that $P_{\delta\delta}$ evaluated at a constant phase angle for a time-dependent simulation evolves in time in much the same manner as $P_{\delta\delta}$ would for a time-independent simulation. As previously mentioned, it is precisely this similarity that enables the relatively simple time-dependent TTCF expressions in Eqs. (2) and (7) to be derived.

The diagonal elements of the pressure tensor, for both the direct and TTCF methods, are plotted in Fig. 3(b). In this case the TTCF data represent the shaded cells in Fig. 2 [i.e., each shaded column represents a point on Fig. 3(b)]. Once again there is excellent agreement between both methods. As expected, P_{xx} and P_{yy} have a period of τ and are out of phase by π, while P_{zz} is weakly oscillatory with period $\pi/2$, even though $\dot{\varepsilon}_{zz}=0$.

Simulations were also performed for a BSF/USF system with $\dot{\varepsilon}_{xx}=-0.5$, $\dot{\varepsilon}_{yy}=0.25$, $\dot{\varepsilon}_{zz}=0.25$. Once again $\omega=12.566$ ($\tau=0.5$), and each NEMD trajectory was run for a total simulation time of 3τ. A total of $10\times3\times140\times50$ trajectories were run. Figure 4(a) displays $P_{\delta\delta}(\varphi_p=0)$ for this system. Once again, agreement between the direct and TTCF methods is excellent, with the direct values statistically superior at these strain rates. Also, as $\dot{\varepsilon}_{yy}=\dot{\varepsilon}_{zz}$, P_{yy} and P_{zz} are identical to within statistical errors.

In Fig. 4(b) the pressures are plotted as functions of time, again displaying excellent agreement between both methods. It is noted here that as TTCF involves time integrations of

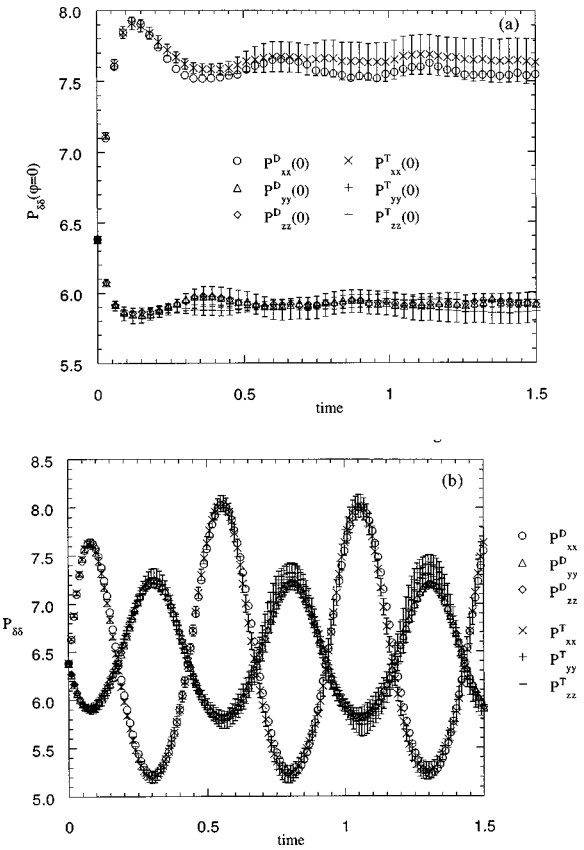

FIG. 4. (a) D and T values of $\langle P_{\delta\delta}[\mathbf{\Gamma}(t;\varphi_p=0)]\rangle$ for a BSF/USF simulation with an applied strain rate of $\dot{\varepsilon}_{xx}=-0.5$, $\dot{\varepsilon}_{yy}=0.25$, $\dot{\varepsilon}_{zz}=0.25$, and frequency of $\omega=12.566$. (b) Direct and TTCF pressures for the system in (a).

correlation functions, statistical errors will propagate as time advances. As these calculations are computationally intensive (a total of 3.15×10^8 time steps for the results in Fig. 4), it is difficult to simulate for total individual trajectory lengths of more than several τ without significant computational resources. The simulations for this study were performed on the CSIRO NEC SX4 vectorizing supercomputer. All simulations were performed using only a single processor. As the TTCF method involves nonequilibrium trajectories that span the entire set of extended phase space, it is ideally suited to parallelization. For maximum efficiency, at each node one processor could be used for each trajectory that spans $\varphi\in[0,2\pi]$. In such a way the time-dependent TTCF calculation would then become equally as efficient as the time-independent TTCF calculation running on a single processor, in that a larger number of nodes are possible, which in turn would improve the overall statistical accuracy of the results.

One of the major advantages of the TTCF method over direct NEMD is to be found in simulations with relatively weak strain rates. In such cases it is well known that direct averaging of phase variables suffers from intolerable signal to noise ratios [12]. Thus, the only practical method currently available is response theory. Note that while other formulations of nonlinear response theory exist, TTCF (both time dependent and time independent) has thus far proved to be the most practical [9–12].

In Figs. 5(a) and 5(b) the results of an oscillating PEF simulation consisting of a total of $5\times2\times2000\times50$ NEMD trajectories are displayed. In this case $\dot{\varepsilon}_{xx}=-0.002$, $\dot{\varepsilon}_{yy}$

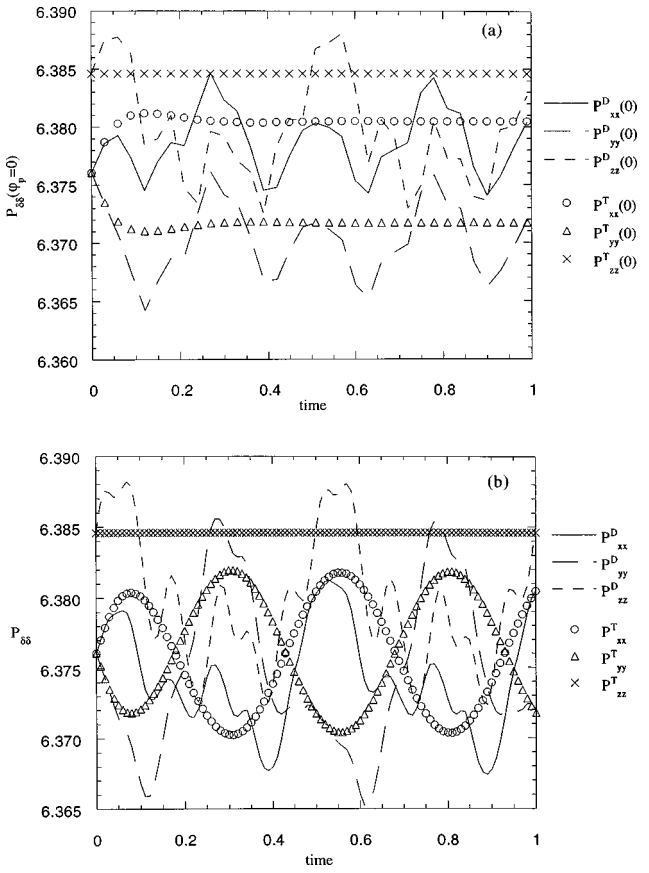

FIG. 5. (a) D and T values of $\langle P_{\delta\delta}[\mathbf{\Gamma}(t;\varphi_p=0)]\rangle$ for a PEF simulation with an applied strain rate of $\dot{\varepsilon}_{xx}=-0.002$, $\dot{\varepsilon}_{yy}=0.002$, $\dot{\varepsilon}_{zz}=0$, and a frequency of $\omega=12.566$. (b) Direct and TTCF pressures for the system in (a).

$=0.002$, $\dot{\varepsilon}_{zz}=0$. The frequency is the same as before, but now the total simulation time per NEMD trajectory is 2τ. It is clear from these figures that for such a low value of $\dot{\varepsilon}$ the TTCF method is able to generate data that does not suffer from the scatter of the direct results, in agreement with the results of Petravic and Evans [11]. Note that on the magnified scale of Fig. 5(a), $\langle P_{xx}(t=0)\rangle=\langle P_{yy}(t=0)\rangle\neq\langle P_{zz}(t=0)\rangle$ due to averaging over the phase-space mappings used. These zero-time (equilibrium) pressures are within error limits of each other (at equilibrium all pressures should be the same in the limit of infinite averaging time).

V. CONCLUSIONS

In this paper, the newly developed time-dependent transient time correlation function theory of Petravic and Evans [11] has been applied to a simple atomic fluid experiencing oscillatory elongational flow. Normal stresses are calculated by the method and compared with direct time-averaged values and excellent agreement is found between both methods, confirming the validity of the theory for generalized time-dependent periodic flows.

At higher values of the applied strain rate direct averaging is seen to be statistically superior to the TTCF results, in contrast to the results of Petravic and Evans [11] who observed similar efficiencies for both methods even at high values of the applied field. It is noted, however, that the work of Petravic and Evans was performed on only a two-particle system, whereas all simulations done for this paper were for a system of 108 particles. It thus appears that direct averaging is still more efficient than the TTCF method for a sufficiently large number of particles at high field strengths. Nevertheless, TTCF is certainly shown to be more efficient than direct averaging at low values of the strain rate, and it is in this region where its superiority is clearly evident for generalized flows. While time-dependent TTCF is computationally intensive, it is highly suited for straightforward parallelization, in which it would be expected to become as computationally efficient as time-independent TTCF calculations are on a single processor machine. Furthermore, as the time-dependent TTCF method spans the entire set of extended phase space, an enormous amount of information is contained within a single set of simulations. Within the current range of computational power available, the time-dependent TTCF method could be extremely valuable for studying small systems, in which the limitations of statistical noise are substantially reduced in comparison to the traditional NEMD procedure of direct time averaging of phase variables.

Note added in proof. Recently, a new method that guarantees unrestricted duration NEMD simulation of time independent planar elongational flow has been implemented. For details see Ref. [13].

ACKNOWLEDGMENT

The author wishes to thank Dr. Janka Petravic for valuable discussions related to this work.

[1] D. M. Heyes, Chem. Phys. **98**, 15 (1985).
[2] M. W. Evans and D. M. Heyes, Mol. Phys. **69**, 241 (1990).
[3] M. N. Hounkonnou, C. Pierleoni, and J.-P. Ryckaert, J. Chem. Phys. **97**, 9335 (1992).
[4] A. Baranyai and P. T. Cummings, J. Chem. Phys. **103**, 10 217 (1995).
[5] M. Kroger, C. Luap, and R. Muller, Macromolecules **30**, 526 (1997).
[6] J. D. Weeks, D. Chandler, and H. C. Andersen, J. Chem. Phys. **54**, 5237 (1971).
[7] B. D. Todd and P. J. Daivis, J. Chem. Phys. **107**, 1617 (1997).
[8] P. J. Daivis and B. D. Todd, Int. J. Thermophys. (to be published).
[9] B. D. Todd, Phys. Rev. E **56**, 6723 (1997).
[10] G. P. Morriss and D. J. Evans, Mol. Phys. **54**, 629 (1985); Phys. Rev. A **35**, 792 (1987); D. J. Evans and G. P. Morriss, Mol. Phys. **61**, 1151 (1987); Phys. Rev. A **38**, 4142 (1988).
[11] J. Petravic and D. J. Evans, Phys. Rev. Lett. **78**, 1199 (1997); J. Petravic and D. J. Evans, Phys. Rev. E **56**, 1207 (1997).
[12] D. J. Evans and G. P. Morriss, *Statistical Mechanics of Nonequilibrium Liquids* (Academic, London, 1990).
[13] B. D. Todd and P. J. Daivis, Phys. Rev. Lett. **81**, 1118 (1998); and (unpublished).